Journal of Vacuum Science and Technology B

RESEARCH ARTICLE | OCTOBER 12 2023

Fabrication of hierarchical nanostructures using binary colloidal nanosphere assembly

Ethan Flores ; Saurav Mohanty ; Andrew Tunell ; Chih-Hao Chang

J. Vac. Sci. Technol. B 41, 062803 (2023)
https://doi.org/10.1116/6.0003027

JVST B
Journal of Vacuum Science & Technology B

ARTICLE

pubs.aip.org/avs/jvb

Fabrication of hierarchical nanostructures using binary colloidal nanosphere assembly

Cite as: J. Vac. Sci. Technol. B **41**, 062803 (2023); doi: 10.1116/6.0003027
Submitted: 31 July 2023 · Accepted: 20 September 2023 ·
Published Online: 12 October 2023

Ethan Flores, Saurav Mohanty, Andrew Tunell, and Chih-Hao Chang[a)]

AFFILIATIONS

Walker Department of Mechanical Engineering, Cockrell School of Engineering, University of Texas at Austin, 301 E Dean Keeton Street, Austin, Texas 78712

Note: This paper is part of the Special Topic Collection: Papers from the 66th International Conference on Electron, Ion and Photon Beam Technology and Nanofabrication (EIPBN 2023).

[a)]**Electronic mail:** chichang@utexas.edu

ABSTRACT

In this paper, we investigate the self-assembly of hierarchical nanostructures using monodispersed nanospheres with two different diameters. Our approach is to use a two-step method where the assembly of larger 200 nm nanospheres is used to direct the assembly of smaller 50 nm particles. This self-assembly technique is based on Langmuir–Blodgett assembly and has low equipment cost when compared with traditional lithography methods. We examine the effects of substrate surface treatment, solution concentration ratio, and spin speeds on the quality of the hierarchical assembly. The fabricated samples are examined using optical and scanning electron microscopy to investigate assembly yield. Various defect types are identified and mitigated by process control. The ability to create more complex assembly can result in smaller features and can enhance the performance of photonics and nanostructured surfaces.

I. INTRODUCTION

Recent developments in top-down nanolithography have helped in pushing the limits of semiconductor manufacturing for next-generation consumer electronics.[1] Such methods include optical, electron-beam,[2] and nanoimprint lithography,[3–5] which can also be used for fabricating integrated chip, microelectromechanical systems (MEMS), and biomedical devices. As these methods are widely used, there are newer upcoming technologies considered next-generation lithography. Some examples include extreme ultraviolet lithography (EUV),[6,7] multibeam electron-beam,[8,9] and two-photon polymerization.[10,11] These advances in nanopatterning have also enabled research in novel nanostructured materials, including nanolattices with better mechanical properties and enhanced stiffness scaling at low density,[12,13] dust-mitigating nanostructured surfaces,[14] and nanophononics with dynamic tunable colors.[15]

In addition to top-down lithography approaches, bottom-up self-assembly techniques can also provide new opportunities because of low equipment cost and high scalability for nanomanufacturing.[1] In this approach, nanoscale elements self-organize into functional geometries with the most energy favorable configuration because of local interactions. Self-assembly approaches are especially useful for applications that require ordered or periodic features, which are typically obtained in these techniques. Self-assembly systems have resulted in assemblies with higher density nanostructures. Examples include self-assembly or directed self-assembly of block copolymers, where two distinct polymer blocks chained by covalent bonds phase separate to form an organized geoemtry.[16–19]

Another example is DNA origami, where precisely designed complementary base pairs have been demonstrated to fold into complex nanoscale assemblies.[20–22] Furthermore, colloidal elements such as nanowires and nanoparticles can be dispersed in a liquid-based solution that can be assembled into functional geometries.[20,23–29] These bottom-up approaches are a promising method to fabricated nanostructures without complex hardware.

One well-known technique is colloidal assembly using monodispersed nanospheres, which results in a hexagonal closed-pack structure on a planar surface to minimize surface area.[30] Convective assembly using a sliding plate is an effective method and provides a facile method to control the evaporation and nanoparticle assembly.[23] Additionally, the assembly of monodispersed nanoparticles can help obtain colloidal crystals, which yields opal structures. The use of

optical lithography and colloidal particle self-assembly[31–34] can also lead to a wide range of nanostructure geometries and help in creating nanolattices,[12,13,35,36] which our group has previously demonstrated. However, most existing research involves the assembly of monodispersed nanospheres, which results in the formation of a periodic pattern. More recent work has examined binary assembly using a heat-assisted assembly[37] and a one-step process where particles are injected into the water for lift-off,[38,39] which has demonstrated a hierarchical structure using microscale particles.[38–40] However, in these works, larger and smaller particles are mixed together in a single solution, which makes independent control difficult. The ability to create more complex assembly can result in smaller features and can enhance the performance of photonics and nanostructured surfaces.[14]

In this work, we present the fabrication of hierarchical nanostructures using a two-step binary colloidal assembly process to create sub-50 nm features by depositing smaller nanoparticles into the voids of an array of larger polystyrene (PS) nanospheres. In this approach, larger nanospheres are assembled at a liquid interface into a hexagonal closed packed assembly and transferred on to a substrate using Langmuir–Blodgett (LB) assembly, which can be used to direct the assembly of the smaller particles in a subsequent step. This creates a hierarchical assembly with an aperture that is smaller than the diameters of the particles used, which can be used as a physical mask for additive and subtractive micromachining or near-field lithography. The advantage of the two-step, layer-by-layer approach is that it allows independent control of layers, which can be more systematically studied. Various process parameters such as surface treatment, surface tension of solution, spin speed, and concentration of nanoparticles are examined to obtain the best packing ratio. The assembly patterns have been analyzed using optical and scanning electron microscopy (SEM) to examine yield and defect modes. The proposed process can create more complex self-assembly patterns and can find applications in nanostructured surfaces and nanophotonic devices.

II. EXPERIMENTAL METHODOLOGY

The advantages of hierarchical assembly are shown in the comparison schematic in Fig. 1. Here, the assembly patterns of monodispersed nanospheres and binary assembly are illustrated. For the monodispersed assembly, nanospheres with a narrow size distribution are used to create a periodic array. In this case, the voids in between the particles typically have dimensions like the sphere diameter.

The proposed two-step assembly process is shown in Fig. 2. Here, polystyrene nanospheres with 200 nm nanospheres in aqueous solution (~2% by concentration, Bangs Laboratories, Inc.) are mixed with ethanol to create a 1:10 ratio solution, shown in Fig. 2(a). The solution is then ultrasonicated to prevent particle aggregation. A silicon wafer is spin-coated with 200 nm nanospheres at 2000 RPM, and this spun-coated wafer is only used to transfer the particles to the final wafer, and then placed into the deionized (DI) water to allow for the nanospheres to rise toward the liquid–air interface, as shown in Figs. 2(b) and 2(c), respectively. A drop of sodium dodecyl sulfate (SDS) is applied to help the nanospheres form a monolayer that is closely packed on the

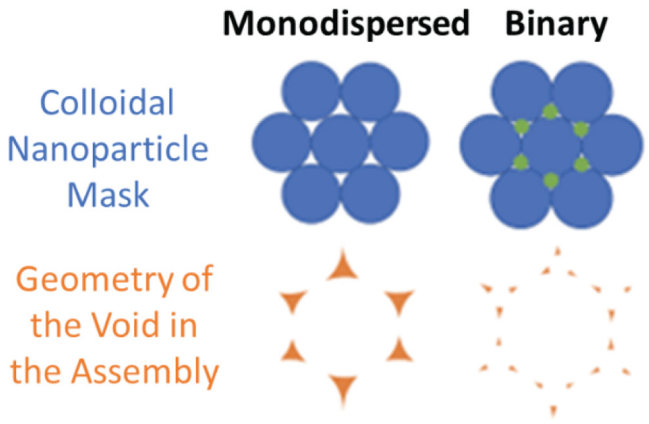

FIG. 1. Comparison of a monodispersed and binary assembly and the void patterns generated. The void for the monolayer assembly is larger than that for the binary assembly.

liquid surface, as shown in Fig. 2(d). Once the monolayer is created, a blank silicon wafer is angled into the water to transfer the nanospheres onto the surface, as shown in Fig. 2(e). The transferred wafer at the bottom of the water dish can either be cleaned to be reused or discarded. Prior to the assembly of the second layer, the surface of the 200 nm nanosphere assembly is treated with an oxygen plasma etcher (Harrick Plasma) at an RF power of 7 W for 5 s to increase the surface energy and improve the hydrophobicity. An aqueous solution of the smaller 50 nm particles (2% concentration, Thermo Scientific) is then prepared with ethanol to create a 1:7 ratio solution and spin-coated on the sample with the 200 nm nanosphere array at 500–2000 RPM, as demonstrated in Fig. 2(f). This process results in a hierarchical structure consisting of binary assembly, as shown in Fig. 2(g), which are then examined using an optical and scanning electron microscope (SEM). In preparation for the SEM, the samples are sputter-coated with 2–3 nm of gold to reduce electron charging.

III. RESULTS AND DISCUSSION

A. First layer assembly of nanosphere array

The quality of the first-layer nanosphere monolayer is examined first to ensure that it can serve as a high-quality template to direct the assembly of the second nanoparticle layer. The goal is to achieve a hexagonal close packed array and examine defects that can occur during the LB assembly process. Note in our experiments that the nanospheres are spin-coated on a silicon wafer and then lifted off when immersed in a petri dish to assemble the colloids on the liquid–air interface. The SEM images of the assembled nanospheres are shown in Fig. 3. Here, the assembled structure shows that a large area assembly of a colloidal crystal is possible. The LB assembly results demonstrate low defect density with a few clustered nanospheres and is used for subsequent assembly of the smaller nanoparticles.

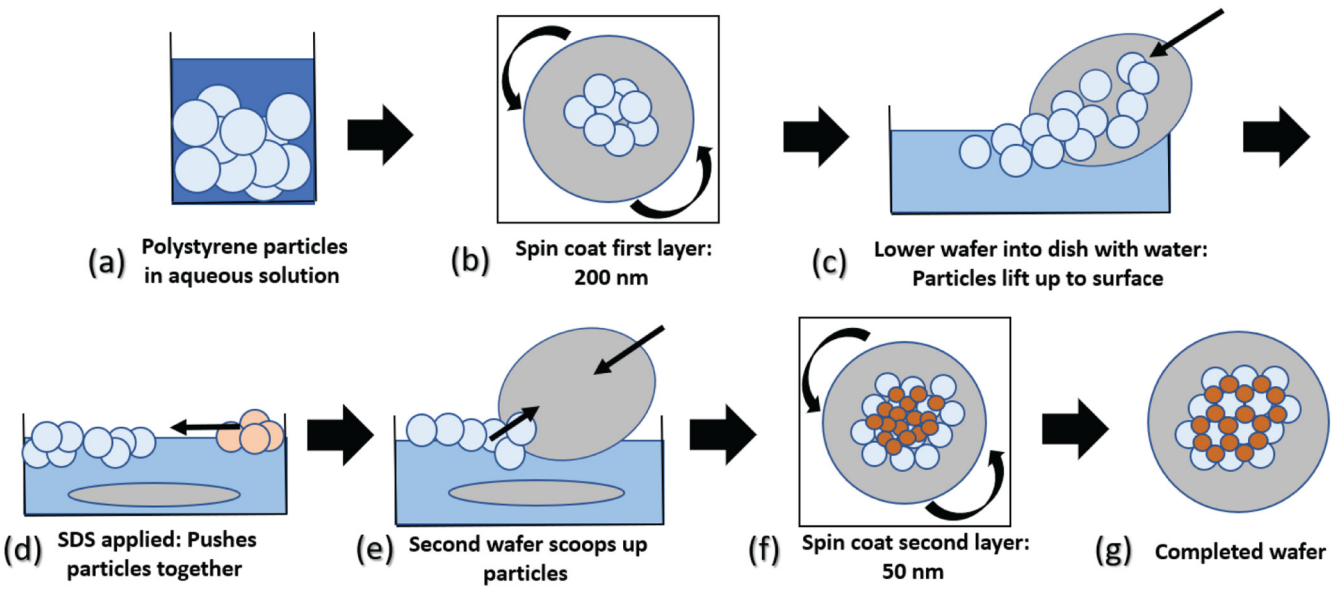

FIG. 2. Schematic of a two-step assembly process. (a) Polystyrene particles mixed in ethanol. (b) Spin-coated first layer of 200 nm nanospheres. (c) Lower spun-coated wafer into dish with water, where particles rise to the water surface. (d) SDS is applied to push particles together to form a monolayer. (e) A blank wafer scoops up a developed monolayer. (f) The dried wafer is spin-coated with a second layer of 50 nm particles. (g) Completed wafer with a binary assembly.

The proposed approach utilizes a separate step to assemble the second layer of smaller nanoparticles with 50 nm diameter, which requires wetting the assembly of the larger nanospheres. It is then important to examine whether wetting the surface of the first layer by a mixture of DI water with ethanol would affect the assembled monolayer. This experiment is meant to replicate the assembly of the smaller nanoparticles during the second assembly step. Figures 4(a) and 4(b) show the optical microscope images of the 200 nm nanosphere samples before and after spincoating with DI water, respectively. As seen in the images, wetting the surface did alter the assembled nanospheres. However, the effect is not significant and only the assembly near the edges is removed, as denoted by the dashed lines. Because the effect is minimal, there is sufficient area to guide the assembly of the second layer in the subsequent step.

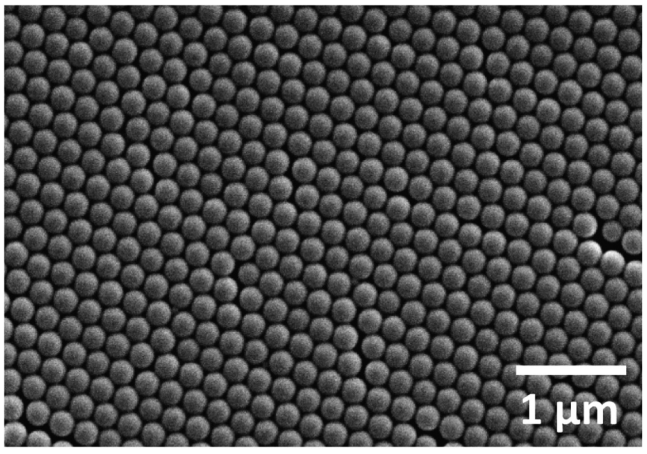

FIG. 3. Top-view SEM images of assembled 200 nm nanospheres in a hexagonal close packed array.

B. Second layer template-directed assembly of nanoparticles

Once the first nanosphere array layer has been assembled to create a hexagonal array, it can serve as a template to direct the assembly of the smaller 50 nm nanoparticles. In this process, the solution of the 50 nm particle in water/ethanol solution is spin-coated on the nanosphere-coated silicon substrate, allowing the smaller particles to fill the voids of the larger spheres. This approach allows the patterning of a binary assembly in a two-step process, which allows the selection of different nanosphere and nanoparticle parameters independently. This allows for the particles to be independently controlled for each step and not risk incapability with each other. Several process parameters can affect the quality of the binary assembly, namely, the nanoparticle concentration and spincoat speed, which are examined further in the following sections.

Initial experiments are performed to investigate the effect of nanoparticle concentration on the quality of the binary assembly, as illustrated in Fig. 5. Here, the solution concentrations varied from 1:1, 1:3, 1:5, and 1:10, as depicted in Figs. 5(a)–5(d), respectively. It can be observed that for high particle concentration, the nanoparticles tend to aggregate and form dense assembly, as

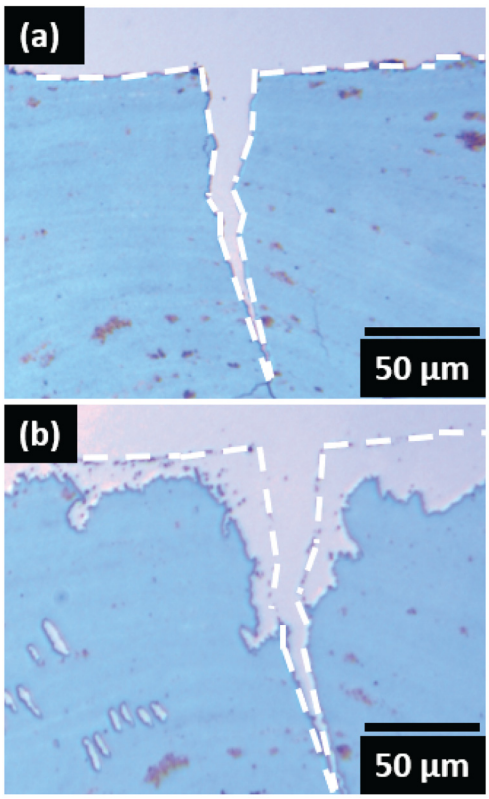

FIG. 4. Optical microscope images of the first layer nanosphere array at the same location on the substrate (a) before and (b) after the sample was wetted with a DI water and ethanol solution.

illustrated in Fig. 5(a) where the particle ratio is 1:1. This ratio created an overabundance of 50 nm particles, which clustered and assembled independently of the underlying 200 nm nanosphere array. At the slightly lower particle concentration of 1:3, as shown in Fig. 5(b), the clustering effects of the particles are reduced but still resulted in multiple layers within the nanosphere voids. A noticeable feature is the ability to see the presence of the particles in the voids. Although the particles did assemble into the voids as desired, there was still a large abundance of the particles that are not well controlled. The particle concentration in the solution was further reduced to 1:5, as shown in Fig. 5(c), where the particles began to fill the voids without overlapping one another. Here, it can be observed that the topological templating effect of the nanosphere array is playing a more prominent role. However, multiple particles still exist within a single nanosphere void, which is undesirable, since they would obstruct the nanoscale aperture of the binary assembly. Further reducing the solution concentration to 1:10, as shown in Fig. 5(d), resulted in fewer nanoparticles. It was noticed that only a few particles assembled within the voids. The particles began to create the desired effects, but there were voids with no particles. Therefore, a slightly increased particle concentration of 1:7 was used for all subsequent experiments.

Another parameter that can affect the assembly of the second nanoparticle layer is the spin-coating speed on the silicon substrates with the 200 nm nanosphere array. To examine this effect, a binary assembly of a 50 nm nanoparticle with a 1:7 ratio solution is spin-coated with 500, 1000, and 1500 RPM, as shown in Fig. 6. Keeping the speeds below 2000 RPM is vital for the particles to assemble into the voids, since the particles tend not to wet the substrate sufficiently at higher spin speeds. The sample with an assembly speed of 500 RPM can be seen in Fig. 6(a). Here, the particles began to assemble into the voids and does not form large clusters. Figure 6(b) depicts the sample with an assembly speed of

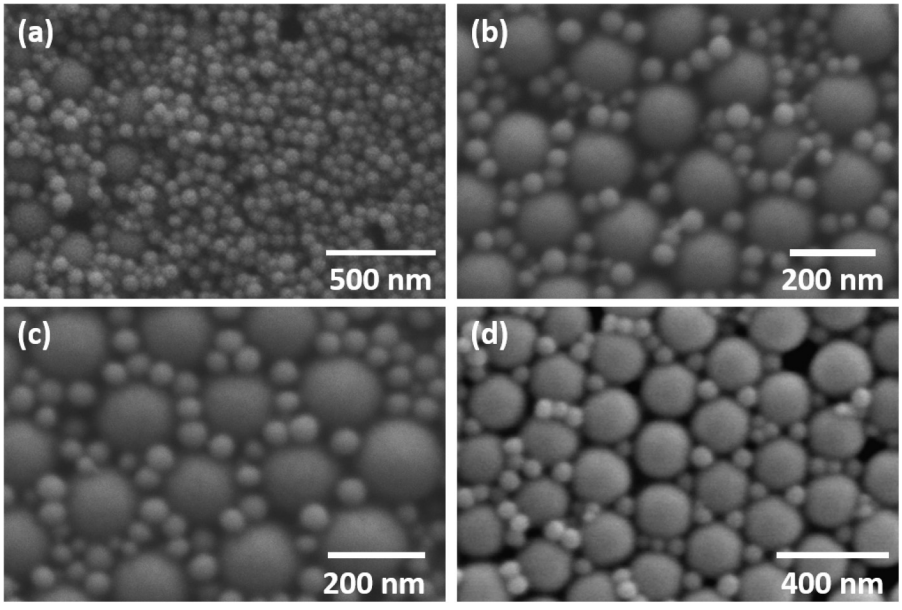

FIG. 5. SEM images of the fabrication results of binary assembly after the second assembly step. (a) 1:1 particle ratio sample showing particle clustering. (b) 1:3 particle ratio sample showing an abundance of particles. (c) 1:5 particle ratio sample showing multiple particles in voids. (d) 1:10 particle ratio sample showing isolated particles in the voids.

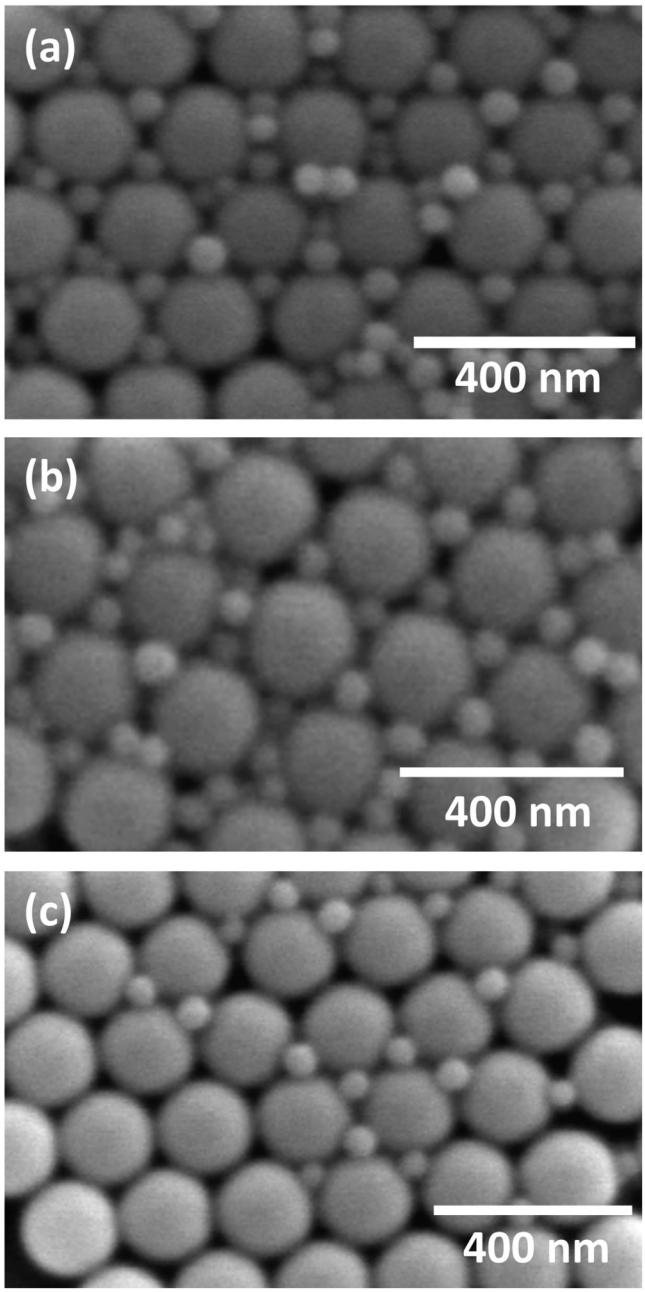

FIG. 6. SEM images of second layer assembly results for 50 nm particles 1:7 ratio. Sample with an assembly speed of (a) 500 RPM, (b) 1000 RPM, and (c) 1500 RPM.

1000 RPM, where the particles assemble in the voids, but some areas showed fewer particles. At a higher assembly speed of 1500 RPM, the sample has higher nanoparticle void density, as shown in Fig. 6(c). It can be determined that slower speeds result in higher assembly yields with more nanoparticles assembling into the nanosphere voids. It is important to note how vital the effects of the assembly speed and nanoparticle concentration are to the quality of the binary assembly.

The results of the nanoparticle concentration and speed experiment indicate that these parameters play a critical role in achieving a higher yield and lower defects. It can be determined that the best assembly results can be obtained with a 1:7 nanoparticle solution ratio and a spin-coating speed of 500 RPM for the second assembly layer. Figure 7(a) depicts the results of the completed binary assembly, which has a pattern area of $1 \times 1\,\mu m^2$. It can be observed that the voids of the first nanosphere array have been greatly reduced by the second particle assembly. A larger assembly of the binary layer over a $2\,\mu m$ by $2\,\mu m$ area can be seen in Figs. 7(b) and 7(c). Here, the total number of available voids in the 200 nm nanosphere array are 99 out of 128, and 67 out of 97 of them are occupied by a single 50 nm particle in the two images, respectively. Therefore, the smaller particle correctly assembled into roughly 77 and 70% of the available voids as desired, respectively. This result demonstrates a promising proof of concept and the process can be improved to further increase yield in the future. The binary assembly can be used as a hierarchical mask for subsequent lift-off, etching, or lithography processes, which is the subject of ongoing studies.

C. Challenges and future work

While the experiments have demonstrated successful assembly of 50 nm nanoparticles into the voids of the 200 nm nanosphere array, assembly defects are a particular challenge. Several defect modes have been identified, as depicted in Fig. 8. Of primary concern is the aggregation of 50 nm particles, which can completely cover the assembled nanosphere monolayer, as shown in Fig. 8(a). The aggregation effect can be mitigated by using an ultrasonication bath, which was used in all experiments. However, particles continue to aggregate over time and the solution must be sonicated right before the assembly process. This is especially problematic for smaller particles due to a high surface area to volume ratio, which can limit the nanoparticle size used. In addition, large assembly voids in the nanosphere array can also form during slower spin-coating speeds, as shown in Fig. 8(b). In these cases, the 50 nm particles would fall into the voids and undercut the nanosphere array. This defect forms in the first layer, and can be mitigated by improving the defect-free area of the nanosphere layer. Another issue is the formation of nanoparticle clusters, which result in overlapping assembly in the nanosphere voids, as seen in Fig. 8(c). This occurrence is related to the solution needing more ultrasonication time or the particle concentration being too high, as discussed earlier. Due to the presence of defects, currently, the binary assembly area is limited to the sub-$3\,\mu m$ range. Future work will examine scaling up the assembly area by mitigation particle aggregations, using particles with lower size distributions, and better control of environmental disturbance during assembly.

Future work will focus on improving the assembly of both the 200 nm nanospheres and the smaller 50 nm nanoparticles. This can be accomplished by a better control of the liquid disturbance and other environmental factors during LB assembly. It can also be noted that the particles used have obvious size variations and using

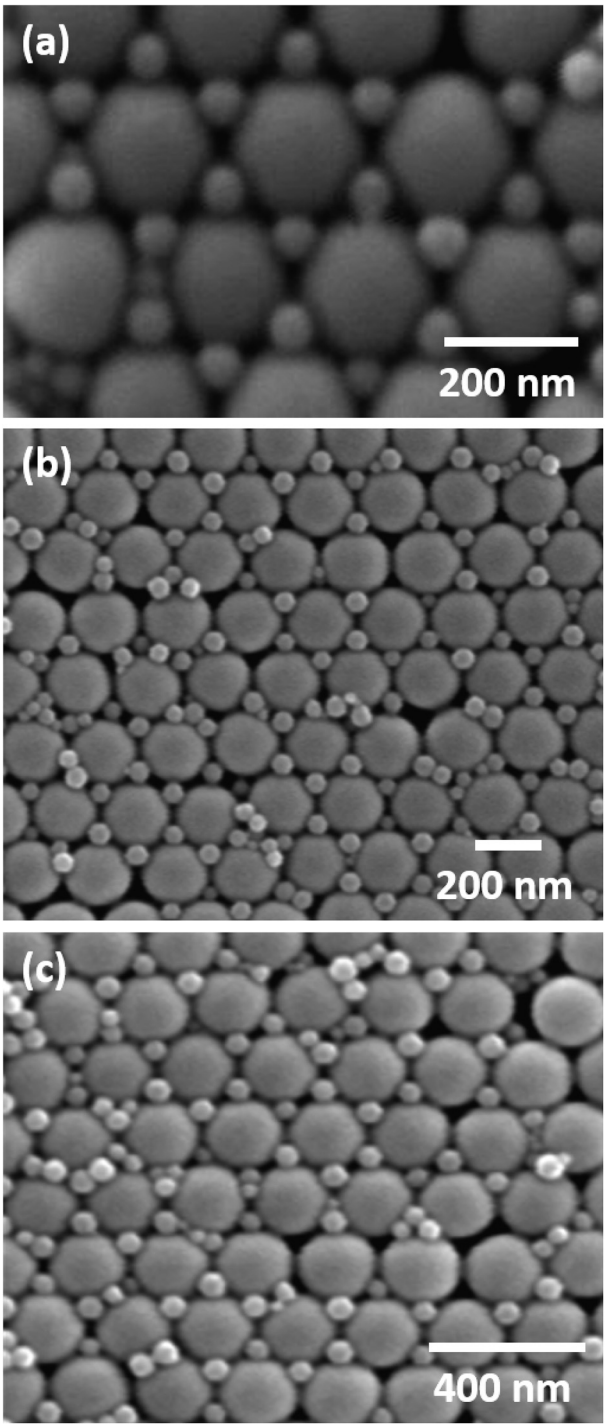

FIG. 7. Binary assembly results. SEM images of (a) completed binary assembly with high magnification. (b) and (c) SEM images of a binary assembly structure at two locations on the sample with 50 nm particles assembling into the voids of the larger nanospheres.

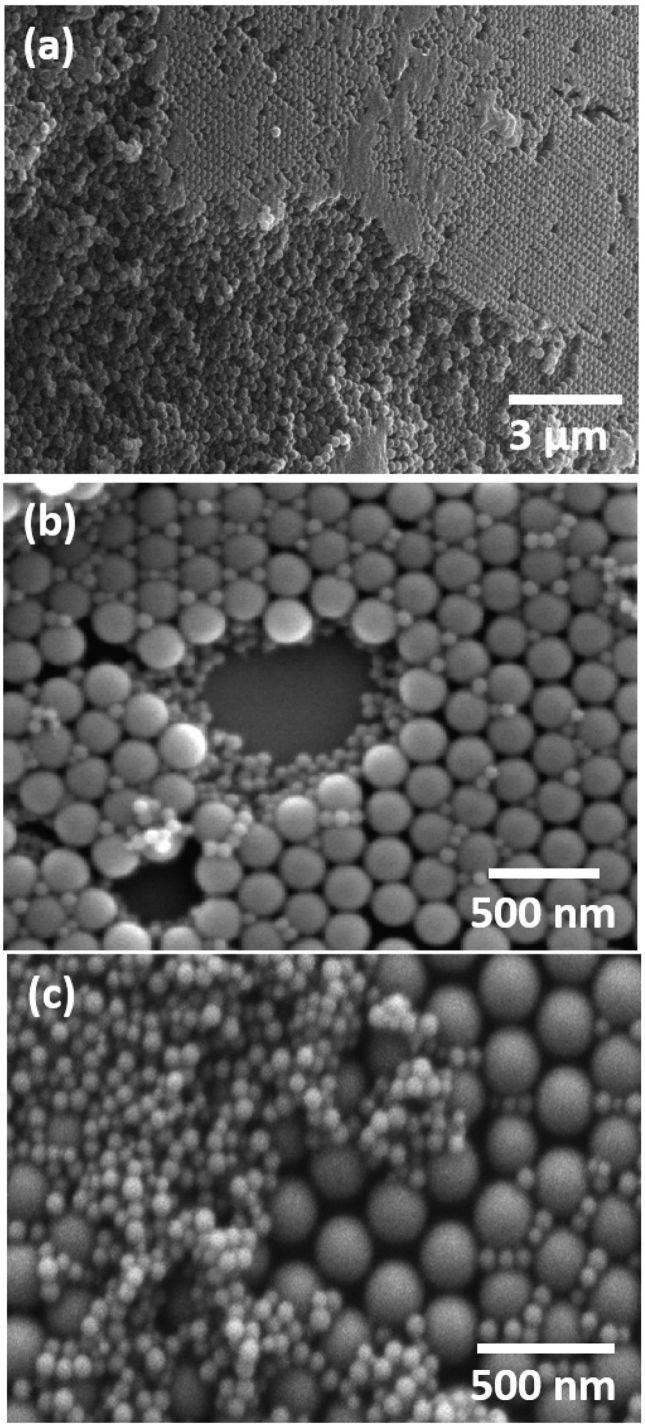

FIG. 8. SEM images of assembly defects due to (a) particle aggregation, (b) assembly void in the 200 nm nanosphere array layer where the 50 nm particles can assemble below, and (c) clustering of particles due to high particle concentration.

colloids with lower size distribution can potentially reduce defect density. We also plan to explore the binary of nanoparticles with various size ratios using the proposed two-step process, which can yield more complex assemblies. In addition, the fabricated binary assembly will be explored as a lift-off or etching mask to transfer the nanoscale aperture into the underlying substrate.

IV. CONCLUSION

This work demonstrates a two-step process to fabricate a hierarchical nanostructure using a binary assembly of 200 nm nanospheres and 50 nm particles. In this process, the larger 200 nm nanosphere array is assembled using LB assembly to create a hexagonal close-packed structure, which serves as a template to guide the assembly of the smaller 50 nm particles. The assembly conditions were found to have a critical influence on the process yield, with the highest quality binary assembly achieved using 1:10 concentration and a spin speed of 2000 RPM for the nanosphere and 1:7 concentration and 500 RPM for the nanoparticles. Other important process steps to reduce defects include plasma treatment to increasing the surface energy and ultrasonication to reduce particle aggregation. The result of this research indicates that finer nanostructure features can be achieved using a binary assembly of nanoparticles, and these features can find applications in enhancing the performance of photonics and nanostructured surfaces.

ACKNOWLEDGMENTS

This work was performed at the UT Austin Texas Materials Institute (TMI), the Nanomanufacturing System for mobile Computing and Energy Technologies (NASCENT), and Texas Nanofabrication Facilities, which is supported by the National Science Foundation (NSF) as part of the National Nanotechnology Coordinated Infrastructure (NNCI) Grant No. NNCI-2025227. The author would like to acknowledge the REU NASCENT program at UT Austin, which supported this research.

AUTHOR DECLARATIONS

Conflicts of Interest

The authors have no conflicts to disclose.

Author Contributions

Ethan Flores: Conceptualization (equal); Data curation (equal); Formal analysis (equal); Investigation (equal); Methodology (equal); Project administration (equal); Software (equal); Validation (equal); Visualization (equal); Writing – original draft (equal); Writing – review & editing (equal). **Saurav Mohanty:** Conceptualization (equal); Investigation (equal); Methodology (equal); Supervision (equal); Visualization (equal); Writing – review & editing (equal). **Andrew Tunell:** Methodology (equal); Supervision (equal); Visualization (equal). **Chih-Hao Chang:** Conceptualization (equal); Funding acquisition (equal); Investigation (equal); Methodology (equal); Project administration (equal); Resources (equal); Supervision (equal); Validation (equal); Visualization (equal); Writing – review & editing (equal).

DATA AVAILABILITY

The data that support the findings of this study are available within the article.

REFERENCES

[1]J. A. Liddle and G. M. Gallatin, ACS Nano **10**, 2995 (2016).
[2]B. J. Lin, J. Micro/Nanolithogr., MEMS, MOEMS **11**, 033011 (2012).
[3]S. Y. Chou, J. Vac. Sci. Technol. B. **14**, 4129 (1996).
[4]L. J. Guo, Adv. Mater. **19**, 495 (2007).
[5]M. Colburn *et al.*, Proc. SPIE. **3676**, 379 (1999).
[6]B. Wu and A. Kumar, J. Vac. Sci. Technol. B. **25**, 1743 (2007).
[7]P. J. Silverman, J. Micro/Nanolithogr., MEMS, MOEMS **4**, 011006 (2005).
[8]T. Kemen, T. Garbowski, and D. Zeidler, Proc. SPIE, **9658**, 965807 (2015).
[9]T. Kemen, M. Malloy, B. Thiel, S. Mikula, W. Denk, G. Dellemann, and D. Zeidler, Proc. SPIE **9424**, 94241U (2015).
[10]V. Hahn, P. Kiefer, T. Frenzel, J. Qu, E. Blasco, C. Barner-Kowollik, and M. Wegener, Adv. Funct. Mater. **30**, 1907795 (2020).
[11]S. K. Saha, D. Wang, V. H. Nguyen, Y. Chang, J. S. Oakdale, and S.-C. Chen, Science **366**, 105 (2019).
[12]A. Bagal *et al.*, Sci. Rep. **7**, 9145 (2017).
[13]X. A. Zhang, A. Bagal, E. C. Dandley, J. Zhao, C. J. Oldham, B.-I. Wu, G. N. Parsons, and C.-H. Chang, Adv. Funct. Mater. **25**, 6644 (2015).
[14]S. S. Lee, L. Micklow, A. Tunell, K.-C. Chien, S. Mohanty, N. Cates, S. Furst, and C.-H. Chang, ACS Appl. Mater. Interfaces **15**, 13678 (2023).
[15]Z. Luo, B. A. Evans, and C.-H. Chang, ACS Nano **13**, 4657 (2019).
[16]Y. Lin *et al.*, Nature **434**, 55 (2005).
[17]M. Park, C. Harrison, P. M. Chaikin, R. A. Register, and D. H. Adamson, Science **276**, 1401 (1997).
[18]G. Krausch and R. Magerle, Adv. Mater. **14**, 1579 (2002).
[19]J. Y. Cheng, C. A. Ross, H. I. Smith, and E. L. Thomas, Adv. Mater. **18**, 2505 (2006).
[20]Y. Y. Pinto, J. D. Le, N. C. Seeman, K. Musier-Forsyth, T. A. Taton, and R. A. Kiehl, Nano Lett. **5**, 2399 (2005).
[21]P. W. K. Rothemund, Nature **440**, 297 (2006).
[22]H. T. Maune, S. P. Han, R. D. Barish, M. Bockrath, W. A. G. Iii, P. W. K. Rothemund, and E. Winfree, Nat. Nanotechnol. **5**, 61 (2010).
[23]B. G. Prevo and O. D. Velev, Langmuir **20**, 2099 (2004).
[24]X. Chen, S. Lenhert, M. Hirtz, N. Lu, H. Fuchs, and L. Chi, Acc. Chem. Res. **40**, 393 (2007).
[25]X. Li and J. F. Gilchrist, Langmuir **32**, 1220 (2016).
[26]O. D. Velev and S. Gupta, Adv. Mater. **21**, 1897 (2009).
[27]Y. Xia, B. Gates, Y. Yin, and Y. Lu, Adv. Mater. **12**, 693 (2000).
[28]N. D. Denkov, O. D. Velev, P. A. Kralchevsky, I. B. Ivanov, H. Yoshimura, and K. Nagayama, Nature **361**, 26 (1993).
[29]M. Grzelczak, J. Vermant, E. M. Furst, and L. M. Liz-Marzán, ACS Nano **4**, 3591 (2010).
[30]J. C. Hulteen and R. P. Van Duyne, J. Vac. Sci. Technol. A **13**, 1553 (1995).
[31]X. A. Zhang, I.-T. Chen, and C.-H. Chang, Nanotechnology **30**, 352002 (2019).
[32]I.-T. Chen, E. Schappell, X. Zhang, and C.-H. Chang, Microsyst. Nanoeng. **6**, 22 (2020).
[33]J.-H. Min, X. A. Zhang, and C.-H. Chang, Opt. Express **24**, A276 (2016).
[34]C.-H. Chang, L. Tian, W. R. Hesse, H. Gao, H. J. Choi, J.-G. Kim, M. Siddiqui, and G. Barbastathis, Nano Lett. **11**, 2533 (2011).
[35]I. T. Chen, Z. Dai, D. T. Lee, Y. A. Chen, G. N. Parsons, and C. H. Chang, Adv. Mater. Interfaces **8**, 2100690 (2021).
[36]V. A. Premnath, I.-T. Chen, K.-C. Chien, and C.-H. Chang, J. Vac. Sci. Technol. B **40**, 062803 (2022).
[37]X. Wang, G. Yi, P. Dong, and S. Chen, Acta Phys. Chim. Sin. **23**, 1707 (2007).
[38]Z. Dai, Y. Li, G. Duan, L. Jia, and W. Cai, ACS Nano **6**, 6706 (2012).
[39]M. Domonkos, P. Demo, and A. Kromka, Crystals **10**, 118 (2020).
[40]F. S. Diba, A. Boden, H. Thissen, M. Bhave, P. Kingshott, and P.-Y. Wang, Adv. Colloid Interface Sci. **261**, 102 (2018).